Commun. Comput. Phys.
doi: 10.4208/cicp.2009.08.206

Vol. **7**, No. 2, pp. 317-332
February 2010

Numerical Investigation of Tumbling Phenomena Based on a Macroscopic Model for Hydrodynamic Nematic Liquid Crystals

Hui Zhang and Qichuan Bai*

School of Mathematical Sciences, Beijing Normal University, Laboratory of Mathematics and Complex Systems, Ministry of Education, Beijing, 100875, China.

Received 28 September 2008; Accepted (in revised version) 13 February 2009

Available online 24 August 2009

Abstract. This paper is concerned with the numerical investigation of a macroscopic model for complex fluids in "1+2" dimension case. We consider the planar pressure driven flow where the direction of the molecules is constrained in the shear plane. The modified Crank-Nicolson finite difference scheme satisfying a discrete energy law will be developed. By using this scheme, it is observed numerically that the direction of the molecules will tumble from the boundary layer and later on the inner layer with a much longer time period. This is consistent with the theoretical prediction. Moreover, we find some complex phenomena, where the tumbling rises from boundary layer and is then embedded into the interior area more clearly when the viscosity coefficient μ of the macro flow has a larger value. The norm of the molecular director **d** will endure greater change as well. This implies that the viscosity of flow plays the role of an accelerator in the whole complex fluids. Comparing these results with the theoretical analysis, we can find that the gradient of the velocity has direct impact on the tumbling phenomena. These results show that the proposed scheme is capable of exploring some physical phenomena embedded in the macro-micro model.

AMS subject classifications: 76T99, 76D05, 65M06

Key words: Complex fluids, energy law, anchoring condition, modified Crank-Nicolson scheme, tumbling.

1 Introduction

The special hydrodynamical properties of complex fluids have attracted many researchers to build up mathematical models and to provide appropriate explanations, see, e.g., [1, 2, 5, 7, 8, 20] and references therein. Doi [2] introduced the Fokker-Plack equation [9]

*Corresponding author. *Email addresses:* hzhang@bnu.edu.cn (H. Zhang), qichuanbai@gmail.com (Q. C. Bai)

coupled with the Navier-Stokes equations, which is a well-known multi-scale model. This model assumed that the fluid is homogeneous in space and excluded volume effect by adopting either Onsager potential [23] or Maier-Saupe potential [2,6,21]. Later, Doi et al. [3] extended the theory to model flows of nonhomogeneous liquid crystal polymers by introducing a long-range intermolecular potential through a mean field calculation. Marrucci and Greco [22] further improved the extended Doi theory and obtained an approximate potential depending on gradients of the second moments of the possibility density function (PDF). Moreover, Wang et al. [24, 25] extended the Doi kinetic model from the rodlike molecule at large aspect ratio to the discotic one at small aspect ratios. Although these models are found useful, the computational cost is large since there are seven variables in the kinetic model (or Fokker-Plack equation of PDF) and the Navier-Stokes-like equations. Therefore, there have been attempts from the macroscopic point of view.

For the macroscopic continuum description of the hydrodynamics of complex fluids, such as the nematic liquid crystals, Ericksen and Leslie derived the following nonlinear coupled system [5,6,14] for those materials with isotropic elastic energies:

$$\mathbf{u}_t+(\mathbf{u}\cdot\nabla)\mathbf{u}+\nabla p=\mu\triangle\mathbf{u}-\lambda\nabla\cdot\tau, \quad \text{in } \Omega, \tag{1.1}$$

$$\nabla\cdot\mathbf{u}=0, \quad \text{in } \Omega, \tag{1.2}$$

$$\mathbf{d}_t+(\mathbf{u}\cdot\nabla)\mathbf{d}-\alpha\kappa\cdot\mathbf{d}-(\alpha-1)\kappa^T\cdot\mathbf{d}=\gamma(\Delta\mathbf{d}-\mathbf{f}(\mathbf{d})), \quad \text{in } \Omega, \tag{1.3}$$

$$\tau=\nabla\mathbf{d}\odot\nabla\mathbf{d}+\alpha(\mathbf{d}\otimes\Delta\mathbf{d}-\mathbf{d}\otimes\mathbf{f})+(\alpha-1)(\Delta\mathbf{d}\otimes\mathbf{d}-\mathbf{f}\otimes\mathbf{d}), \tag{1.4}$$

where $\mathbf{u}$ represents the velocity of the liquid crystal flow, p the pressure, $\kappa=(\nabla\mathbf{u})^T$, and $\mathbf{d}$ the orientation of the liquid crystal molecules. The domain $\Omega\subset\mathbb{R}^n$ is a bounded domain. The induced tensor τ shows the impact of the microstructure on the macro fluid while the coupled term of velocity and director in (1.3) shows impact of the fluid on the microstructure. In Eq. (1.4), the term $\nabla\mathbf{d}\odot\nabla\mathbf{d}$ denotes a 3×3 matrix whose (i,j)-th entry is given by $\mathbf{d}_{x_i}\cdot\mathbf{d}_{x_j}$, for $1\le i,j\le3$, while the term $\mathbf{d}\otimes\Delta\mathbf{d}$ also denotes a 3×3 matrix whose (i,j)-th entry is given by $d_i\Delta d_j$. Here, μ is the viscosity coefficient of the macro fluid and γ is the diffusive parameter for the molecular direction $\mathbf{d}$. Moreover, λ is the competition ratio of the kinetic energy and the elastic energy, $\alpha\in[0,1]$ is a shape parameter of the molecule, and $\mathbf{f}(\mathbf{d})$ may be seen as a penalty function to approximate the constraint $|\mathbf{d}|=1$. In this paper, we choose

$$\mathbf{f}(\mathbf{d})=\nabla\mathbf{F}(\mathbf{d}), \tag{1.5a}$$

where

$$\mathbf{F}(\mathbf{d})=\frac{1}{\epsilon^2}(|\mathbf{d}|^2-1)^2, \tag{1.5b}$$

where the parameter ϵ is the penalty parameter. The transport of the director, $\mathbf{d}_t+(\mathbf{u}\cdot\nabla)\mathbf{d}-\alpha\kappa\cdot\mathbf{d}-(\alpha-1)\kappa^T\cdot\mathbf{d}$ reflects the microscopic picture of those ellipsoid shaped molecules moving in Stokes fluids with no slip boundary conditions on the particle surface [10, 11]. It presents an effective stretching effect on the director $\mathbf{d}$, the reader may refer to [17] for the detail.

The system (1.1)-(1.4) with the no-slip boundary condition

$$\mathbf{u}=0 \quad \text{on } \partial\Omega, \tag{1.6}$$

satisfies the energy law:

$$\frac{1}{2}\frac{d}{dt}\int_\Omega \Big(|\mathbf{u}|^2+\lambda(|\nabla \mathbf{d}|^2+2F(\mathbf{d}))\Big)dx=-\int_\Omega \Big(\mu|\nabla \mathbf{u}|^2+\lambda\gamma|\triangle \mathbf{d}-\mathbf{f}(\mathbf{d})|^2\Big)dx. \tag{1.7}$$

In fact, multiplying (1.1) by $\mathbf{u}$ and integrating the resulting equation over Ω, multiplying (1.3) by $\lambda(-\triangle \mathbf{d}+f(\mathbf{d}))$ and integrating the resulting equation over Ω, and then adding the two results, we obtain

$$\begin{aligned}&(\mathbf{u},\mathbf{u}_t)+(\mathbf{u}\cdot\nabla\mathbf{u},\mathbf{u})-\mu(\triangle\mathbf{u},\mathbf{u})+(\nabla p,\mathbf{u})+\lambda(\tau,\mathbf{u})\\&\quad+\lambda(\mathbf{d}_t,-\triangle\mathbf{d}+f(\mathbf{d}))+\lambda(\mathbf{u}\cdot\nabla\mathbf{d},-\triangle\mathbf{d}+f(\mathbf{d}))\\&\quad+\lambda([\alpha\kappa+(\alpha-1)\kappa^T]\cdot\mathbf{d},\triangle\mathbf{d}-f(\mathbf{d}))+\lambda\gamma\|\triangle\mathbf{d}-f(\mathbf{d})\|^2=0,\end{aligned} \tag{1.8}$$

where $(\cdot,\cdot)$ denotes the usual inner product of $L^2(\Omega)$ and $\|\cdot\|$ denotes the corresponding L^2-norm. Using (1.2), (1.5)-(1.6), and the fact that

$$\nabla\cdot(\nabla\mathbf{d}\odot\nabla\mathbf{d})=\nabla\Big(\frac{|\nabla\mathbf{d}|^2}{2}\Big)+\triangle\mathbf{d}\cdot\nabla\mathbf{d},$$

yield

$$(\mathbf{u}\cdot\nabla\mathbf{u},\mathbf{u})=(\nabla p,\mathbf{u})=(\mathbf{u}\cdot\nabla\mathbf{d},f(\mathbf{d}))=\Big(\mathbf{u},\nabla(\frac{|\nabla\mathbf{d}|^2}{2})\Big)=0. \tag{1.9}$$

Thus, by (1.4), we obtain (1.7). This energy law shows that this system is dissipative. The analytical results in [13–15] indicate that these energy laws are particularly important when singularities are involved in studying the hydrodynamical motions of these crystal materials. The singularities are those energetically admissible ones. There have been several previous attempts to track the physical singularities in numerical simulations [4,13,16–20]. For example, a spectral approach is studied in [4], and the operator-splitting methods are investigated for a liquid crystal model [7,8]. In [18], a mixed finite element method is applied to the system to avoid using the C^1 elements. Recently in [16] a direct weak formulation is introduced and a C^0 finite element method is used. Lin et al. [17] used the C^0 finite element scheme to solve the whole system and revealed how the defect is evolved. The main contribution in [17] was to construct numerical schemes satisfying energy laws to track singularities. In this work, we will try to reveal some basic physical phenomena such as tumbling with less computational efforts. We will consider the model in the "1+2" dimension case by using a finite difference scheme.

Now we state the "1+2" dimension problem. A pressure driven flow acrossing the y-z plane is given as in Fig. 1. Incompressibility indicates $\mathbf{u}=(0,V(z),0)$, $z\in\Omega=(0,\pi)$.

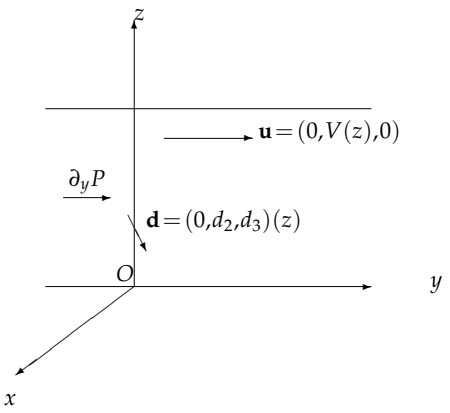

Figure 1: A pressure driven flow acrossing the y-z plane.

We would like to study the velocity $V(z)$ and the orientation $\mathbf{d}$ which is confined in the y-z plane, i.e., $\mathbf{d}$=$(0,d_2,d_3)(z)$.

We set following conditions: $\partial_y P = C$ $(constant)$, no-slip boundary condition for V, i.e., $V|_{\partial\Omega} = 0$, and anchoring condition for $\mathbf{d}$, i.e., $\mathbf{d}$ is a given vector on the boundary. Then (1.1)-(1.4) can be rewritten as follows:

$$\partial_t V + \partial_y P = \mu \partial_{zz} V - \lambda \partial_z \tau_{31}, \qquad \text{in}\,(0,\pi), \tag{1.10}$$

$$\partial_t d_2 - \alpha \partial_z V d_3 = \gamma(\Delta d_2 - f_2(\mathbf{d})), \qquad \text{in}\,(0,\pi), \tag{1.11}$$

$$\partial_t d_3 - (\alpha-1)\partial_z V d_2 = \gamma(\Delta d_3 - f_3(\mathbf{d})), \qquad \text{in}\,(0,\pi), \tag{1.12}$$

$$\tau_{31} = \alpha d_3(\Delta d_2 - f_2) + (\alpha-1) d_2(\Delta d_3 - f_3), \qquad \text{in}\,(0,\pi), \tag{1.13}$$

where $\mathbf{f}(\mathbf{d})$ is the same as in (1.5). The detailed initial conditions will be given in the next section.

Firstly, we point out that the vector $\mathbf{d}$ in the system (1.10)-(1.13) would tumble in the shear plane under some special case. Assume $\gamma = 0$ and $\partial_z V = \omega$ which is a positive constant. It follows from Eqs. (1.11) and (1.12) that

$$\partial_t d_2 - (\alpha-1)\omega d_3 = 0,$$
$$\partial_t d_3 - \alpha\omega d_2 = 0.$$

A combination of these two equations yields

$$\partial_{tt} d_3 - \alpha(\alpha-1)\omega^2 d_3 = 0.$$

The general solution of this equation is

$$d_3 = A\cos\sqrt{\alpha(\alpha-1)\omega^2}\,t + B\sin\sqrt{\alpha(\alpha-1)\omega^2}\,t,$$

where A and B are two parameters. This shows that d_3 is periodic with respect to t. Using the same method, it can be shown that d_2 is also periodic and $\mathbf{d}$ is uniformly tumbling at

each point $z\in(0,\pi)$. This theoretical analysis guides us partially to numerically investigate the tumbling phenomena of the molecular director **d**. Here our goal is to investigate the behavior of the vector **d** when the parameter γ is not zero and $\partial_z V$ is not a constant in (1.10)-(1.13).

In this work, we will make some numerical investigations on the model (1.10)-(1.13). We construct a simple finite difference scheme satisfying a corresponding discrete energy law. It is expected that the physical singularities can be captured by using this scheme. It is pointed out that the scheme to be employed is easier than the finite element method although they use similar computational costs in numerical simulations. We use the fixed point iteration during the linearization and implement the algorithm on a staggered grid. We find the appropriate interval for the penalty parameter ϵ to ensure that the discrete energy declines because theoretically the energy always decline for any positive value of the parameter ϵ. Then we give some numerical examples which show that the molecules will tumble first in the boundary layer and later on the inner layer with a longer time period. It is shown by numerical simulations that the tumbling phenomena can be observed more clearly when the viscosity coefficient μ is larger. We also find that the velocity gradient is a direct driving factor through a comparison with the theoretical analysis earlier.

The rest of this paper is arranged as follows. In Section 2, we present a discrete system in finite difference form and prove that this scheme satisfies an energy law. Implementation issues are discussed in Section 3, including the fixed point iteration strategy. In Section 4, we present our numerical results and discussions. We draw a conclusion in the final section.

2 The discrete system and energy law

In this section, we give a finite difference approach based on the modified Crank-Nicolson scheme to solve the "1+2' dimension problem. The scheme is similar to its counter part in finite element form in [17]. We also present a corresponding discrete energy law which is of great importance both theoretically and numerically.

Divide the interval $(0,\pi)$ into N parts, and let $\Delta h=\pi/N$. A mid-point finite difference scheme similar to its counter part in the finite element scheme [17] is presented below:

$$V_t^{n+1}+\partial_y P=\mu\Delta V^{n+\frac{1}{2}}-\frac{\lambda}{\gamma}\partial_z\Big(\alpha d_3^{n,n-1}(d_{2t}-\alpha\frac{\partial V^{n+\frac{1}{2}}}{\partial z}d_3^{n,n-1}) + (\alpha-1)d_2^{n,n-1}(d_{3t}-(\alpha-1)\frac{\partial V^{n+\frac{1}{2}}}{\partial z}d_2^{n,n-1})\Big), \tag{2.1}$$

$$d_{2t}^{n+1}-\alpha\frac{\partial V^{n+\frac{1}{2}}}{\partial z}d_3^{n,n-1}=\gamma\Big(\Delta d_2^{n+\frac{1}{2}}-f_2(\mathbf{d})\Big), \tag{2.2}$$

$$d_{3t}^{n+1}-(\alpha-1)\frac{\partial V^{n+\frac{1}{2}}}{\partial z}d_2^{n,n-1}=\gamma\Big(\Delta d_3^{n+\frac{1}{2}}-f_3(\mathbf{d})\Big), \tag{2.3}$$

where V^n stands for a $1\times(N+1)$ vector when $t=n\Delta t$, and $V_i=V(i\Delta h)$,

$$V_t^{n+1}=\frac{V^{n+1}-V^n}{\Delta t},\quad V^{n+\frac{1}{2}}=\frac{V^{n+1}+V^n}{2},\quad (\Delta V)_i=\frac{V_{i+1}+V_{i-1}-2V_i}{\Delta h^2}, \tag{2.4a}$$

$$\frac{\partial V}{\partial z}=\frac{V_{i+1}-V_i}{\Delta h},\qquad d_2^{n,n-1}=\frac{3d_2^n-d_2^{n-1}}{2}; \tag{2.4b}$$

other terms in (2.1)-(2.3) have similar definition. Moreover, $\mathbf{f}(\mathbf{d})$ allows different forms to be discussed below. To avoid having too many derivatives, we here replace the terms $\Delta\mathbf{d}-\mathbf{f}$ in τ with the corresponding part in Eq. (2.3) and $\mathbf{d}^{n,n-1}$ is an approximation of $\mathbf{d}^{n+\frac{1}{2}}$ for $\mathbf{d}=(d_2,d_3)$. The discrete energy law is anticipated to be

$$\begin{aligned}&\left(\frac{1}{2}\|V^{n+1}\|_{l^2}^2+\frac{\gamma}{2}\|\nabla\mathbf{d}^{n+1}\|_{l^2}^2+\gamma\|F(\mathbf{d}^{n+1})\|_{l^1}\right)_t\\&=-\left(\mu\|\nabla V^{n+\frac{1}{2}}\|_{l^2}^2+\frac{\lambda}{\gamma}\|\mathbf{d}_t^{n+1}+D_\alpha(V^{n+\frac{1}{2}})d^{n,n-1}\|_{l^2}^2+(\partial_yP\cdot V)_l\right),\end{aligned} \tag{2.5}$$

where we have some notation as follows

$$\|V\|_{l^2}^2=\sum_{i=1}^{N-1}V_i^2,\quad \|\nabla V\|_{l^2}^2=\frac{1}{\Delta h^2}\sum_{i=1}^{N}(V_i-V_{i-1})^2, \tag{2.6a}$$

$$\|\nabla\mathbf{d}^{n+1}\|_{l^2}^2=\|\nabla d_2^{n+1}\|_{l^2}^2+\|\nabla d_3^{n+1}\|_{l^2}^2, \tag{2.6b}$$

$$\|F(\mathbf{d}^{n+1})\|_{l^1}=\sum_{i=1}^{N-1}|F(\mathbf{d}^{n+1})|,\quad (\partial_yP\cdot V)_l=\sum_{i=1}^{N-1}\partial_yP\times V[i], \tag{2.6c}$$

$$D_\alpha(V)\mathbf{d}=\left(\alpha\frac{\partial V}{\partial z}d_3,(\alpha-1)\frac{\partial V}{\partial z}d_2\right), \tag{2.6d}$$

where d_2 and d_3 share a similar definition with V.

Compared with the energy law in [17], we have an extra $(\partial_yP\cdot V)_l$ term in Eq. (2.5). This is because we assume ∂_yP is a constant instead of a system variable in our model. Thus the term $(\partial_yP\cdot V)_l$ will appear to measure the external impact. When the imposed pressure gradient ∂_yP equals to zero, the discrete energy would decline according to the energy law which indicates that the isolated system is dissipative.

Numerically, it is a criterion for us to recognize whether we are giving right numerical solutions for the complex discrete system. When ∂_yP equals zero, the total energy should decline. Even when ∂_yP does not equal to zero in our numerical tests, if we take the initial condition for velocity zero and the term $(\partial_yP\cdot V)_l$ positive, then this will accelerate the declining of total energy. The numerical tests show that when the energy does not decline, the solution is weird which we think is not physically reasonable. So we can use energy declining property to check whether the discrete system is appropriately solved or whether our parameters are well chosen. Now we will state and prove our main theorem in the following.

Theorem 2.1. *The energy law* (2.5) *is satisfied under following conditions:*

C1. V has non-slip boundary condition, i.e., $V_0 = V_N = 0$;

C2. $\boldsymbol{d}$ *has anchoring boundary condition, i.e.,* $\boldsymbol{d}$ *is independent of time on the boundary, i.e.,*

$$d_0^n = d_0^{n+1} = d_0, \quad d_N^n = d_N^{n+1} = d_N;$$

C3. $\boldsymbol{f(d)}$ *bears a modified Crank-Nicolson scheme in the following sense:*

$$\boldsymbol{f}^n(\boldsymbol{d}) = \frac{4}{\epsilon^2}\frac{(|\boldsymbol{d}_h^{n+1}|^2-1)+(|\boldsymbol{d}_h^n|^2-1)}{2}\frac{\boldsymbol{d}_h^{n+1}+\boldsymbol{d}_h^n}{2}. \tag{2.7}$$

The proof can be obtained using the following.

Let V_t, $V^{n+\frac{1}{2}}$, $\mathbf{d}^{n+\frac{1}{2}}$ etc are defined by (2.1)-(2.4), and F is defined by (1.5). Then

$$V_t^{n+1}\cdot V^{n+\frac{1}{2}} = \Big(\Big\|V^{n+1}\Big\|^2\Big)_t, \quad \Delta V^{n+\frac{1}{2}}\cdot V^{n+\frac{1}{2}} = -\|\nabla V^{n+\frac{1}{2}}\|_{L^2}^2; \tag{2.8}$$

$$\Delta\mathbf{d}^{n+\frac{1}{2}}\cdot\mathbf{d}_t^{n+1} = -\frac{1}{2}\Big(\|\nabla\mathbf{d}^{n+1}\|_{l^2}^2\Big)_t; \tag{2.9}$$

$$\mathbf{f}(\mathbf{d})\cdot\mathbf{d}_t^{n+1} = (|F^{n+1}(\mathbf{d})|)_t, \tag{2.10}$$

where $\mathbf{f}^n(\mathbf{d})$ is defined by (2.7).

The detailed proof (2.8)-(2.9) can be found in [12], and (2.10) was derived in [17].

Summing both sides of $((2.1)\times V^{n+\frac{1}{2}} + \frac{\lambda}{\gamma}((2.2)\times d_{2_t}^{n+1} + (2.3)\times d_{3_t}^{n+1}))$, we can find that some terms will eliminate and the rest terms form the energy law (2.5). On the other hand, the coupled term $\partial_z V\cdot\mathbf{d}$ appearing in Eqs. (2.2) and (2.3) is the convection term for the molecule direction, i.e., it take into account the impact of the fluid on the microstructure. According to Newton's third law, i.e., all forces in the universe occur in equal but oppositely directed pairs, it is natural to expect that we can eliminate these terms and get the desired equality.

Proof of Theorem 2.1. We first prove the result $(\partial_z A)\cdot B = -A\cdot(\partial_z B), \forall A, B\in\mathbb{R}^n$ when the condition **C1** is satisfied:

$$\begin{aligned}(\partial_z A)\cdot B &= \sum_{i=0}^{N-1}\frac{A_{i+1}-A_i}{\Delta h}B_i\\ &= -\frac{1}{\Delta h}\Big(\sum_{i=1}^{N-1}A_i(B_i-B_{i-1}) - A_0B_0 + A_NB_N\Big)\\ &= -A\cdot(\partial_z B),\end{aligned}$$

provided that $A_0B_0 - A_NB_N = 0$. Now taking $B = V^{n+\frac{1}{2}}$ and

$$A = \alpha d_3^{n,n-1}\Big(d_{2t} - \alpha\frac{\partial V^{n+\frac{1}{2}}}{\partial z}d_3^{n,n-1}\Big) + (\alpha-1)d_2^{n,n-1}\Big(d_{3t} - (\alpha-1)\frac{\partial V^{n+\frac{1}{2}}}{\partial z}d_2^{n,n-1}\Big),$$

we have

$$\begin{aligned}
&\frac{\lambda}{\gamma}\partial_z\Big(\alpha d_3^{n,n-1}(d_{2_t}^{n+1}-\alpha\frac{\partial V^{n+\frac{1}{2}}}{\partial z}d_3^{n,n-1})\\
&\quad+(\alpha-1)d_2^{n,n-1}(d_{3_t}^{n+1}-(\alpha-1)\frac{\partial V^{n+\frac{1}{2}}}{\partial z}d_2^{n,n-1})\Big)V^{n+\frac{1}{2}}\\
=&-\frac{\lambda}{\gamma}\Big((\alpha\frac{\partial V^{n+\frac{1}{2}}}{\partial z}d_3^{n,n-1})d_{2_t}^{n+1}+(\alpha-1)\frac{\partial V^{n+\frac{1}{2}}}{\partial z}d_2^{n,n-1}d_{3_t}^{n+1}\\
&-(\alpha\frac{\partial V^{n+\frac{1}{2}}}{\partial z}d_3^{n,n-1})^2-((\alpha-1)\frac{\partial V^{n+\frac{1}{2}}}{\partial z}d_2^{n,n-1})^2\Big).
\end{aligned}$$

Next we will prove the energy law (2.5) by calculating $(2.1)\times V^{n+\frac{1}{2}}+\frac{\lambda}{\gamma}((2.2)\times d_{2_t}^{n+1}+(2.3)\times d_{3_t}^{n+1})$ and using (2.8)-(2.10). It can be verified that the left-hand side of $(2.1)\times V^{n+\frac{1}{2}}+\frac{\lambda}{\gamma}((2.2)\times d_{2_t}^{n+1}+(2.3)\times d_{3_t}^{n+1})$ is

$$\begin{aligned}
&\frac{1}{2}\big(\|V^{n+1}\|_{l^2}^2\big)_t+(\partial_y P\cdot V)_l\\
&\quad+\frac{\lambda}{\gamma}\Big(\|\mathbf{d}_t^{n+1}\|_l^2-\alpha\frac{\partial V^{n+\frac{1}{2}}}{\partial z}d_3^{n,n-1}d_{2_t}^{n+1}-(\alpha-1)\frac{\partial V^{n+\frac{1}{2}}}{\partial z}d_2^{n,n-1}d_{3_t}^{n+1}\Big).
\end{aligned}\tag{2.11}$$

Also, the corresponding right-hand side is of the form

$$\begin{aligned}
&-\mu\|\nabla V^{n+1}\|_{l^2}^2-\frac{\lambda}{\gamma}\Big((\alpha\frac{\partial V^{n+\frac{1}{2}}}{\partial z}d_3^{n,n-1})d_{2_t}^{n+1}+((\alpha-1)\frac{\partial V^{n+\frac{1}{2}}}{\partial z}d_2^{n,n-1})d_{3_t}^{n+1}\\
&\quad-(\alpha\frac{\partial V^{n+\frac{1}{2}}}{\partial z}d_3^{n,n-1})^2-((\alpha-1)\frac{\partial V^{n+\frac{1}{2}}}{\partial z}d_2^{n,n-1})^2\Big)-\frac{\gamma}{2}\big(\|\nabla d^{n+1}\|_{l^2}^2\big)_t-\gamma(|F(\mathbf{d})|)_t.
\end{aligned}\tag{2.12}$$

Combining (2.11) and (2.12) yields (2.5). □

3 Implementation issues

In this section we will show how to solve the system (2.1)-(2.3). In our modified Crank-Nicolson scheme, we adopt the fix point iteration to the nonlinearity of the $\mathbf{f}(\mathbf{d})$ term during the linearization, which is introduced by Lin et al. in [17]. By taking this process, we are able to decompose the overall highly non-linear system into two linear parts, i.e., the velocity V part and the director $\mathbf{d}$ part. We solve these two parts alternatively. Finally, we can get a sequence of the approximation of $(V,\mathbf{d})$ on each time step. When this sequence converges to one point, we mark that point as our desired solution. We realize this algorithm on a staggered mesh to increase the stability of the algorithm.

Let V_s be the approximation of V^{n+1} during the fixed point iteration. At each time step, given V^n, we start from $s=1$ and set $V_{s-1}=V^n,\mathbf{d}_{s-1}=\mathbf{d}^n$. We use the following

scheme to compute $V_1, V_2, \cdots$ and $\mathbf{d}_1, \mathbf{d}_2, \cdots$ until $\|V_s - V_{s-1}\| + \|\mathbf{d}_s - \mathbf{d}_{s-1}\|$ becomes small enough. Then we find the fixed points of this time step and use the final values as V^{n+1} and $\mathbf{d}^{n+1}$. The discrete scheme is as follows:

$$(V_s)_t + \partial_y P = \mu\Delta\frac{V^n + V_s}{2} - \frac{\lambda}{\gamma}\partial_z\tau_{31}, \tag{3.1}$$

$$(d_{2s})_t - \frac{\alpha}{2}\frac{\partial(V^n + V_{s-1})}{\partial z}d_3^{n,n-1} = \gamma\Big(\Delta\frac{d_2^n + d_{2s}}{2} - f_2(\mathbf{d})\Big), \tag{3.2}$$

$$(d_{3s})_t - \frac{\alpha-1}{2}\frac{\partial(V^n + V_{s-1})}{\partial z}d_2^{n,n-1} = \gamma\Big(\Delta\frac{d_3^n + d_{3s}}{2} - f_3(\mathbf{d})\Big), \tag{3.3}$$

$$\begin{aligned}\tau_{31} = {}& \alpha d_3^{n,n-1}\Big((d_{2s})_t - \frac{\alpha}{2}\frac{\partial(V^n + V_{s-1})}{\partial z}d_3^{n,n-1}\Big)\\ & + (\alpha-1)d_2^{n,n-1}\Big((d_{3s})_t - \frac{\alpha-1}{2}\frac{\partial(V^n + V_{s-1})}{\partial z}d_2^{n,n-1}\Big),\end{aligned} \tag{3.4}$$

where

$$\mathbf{f}(\mathbf{d}) = \frac{4}{\epsilon^2}\frac{(|\mathbf{d}_{s-1}|^2 - 1) + (|\mathbf{d}^n|^2 - 1)}{2}\frac{\mathbf{d}_{s-1} + \mathbf{d}^n}{2}, \quad (V_s)_t = \frac{V_s - V^n}{\triangle t},$$

and $(d_{2s})_t$ and $(d_{2s})_t$ are defined similarly to $(V_s)_t$. Moreover, $\mathbf{d}^{n,n-1}$ is replaced by $(\mathbf{d}_n + \mathbf{d}_{s-1})/2$ in order to obtain a time independent decomposition.

Remark 3.1. To improve the stability of the numerical scheme, we adopt a staggered mesh. We assume that the unknown spatial area is $(0, N\triangle h)$, where $N+1$ is the number of total grid points, and $\triangle h$ is the space step. We compute from $t=0$ until $t = T\triangle t$. We set the value of $\mathbf{d} = (d_2, d_3)$ on the integer points and mark them as $\mathbf{d}[0], \mathbf{d}[1], \cdots, \mathbf{d}[N]$. While we set the value of V on the half points and mark them as $V[0], V[1], \cdots, V[N], V[N+1]$ (see Fig. 2). Here $V[0], V[N+1]$ are values at two ghost points imposed to ensure that $V = 0$ on the boundary. Thus

$$\begin{aligned}&V[0] + V[1] = 0, \quad V[N] + V[N+1] = 0,\\ &\frac{\partial V}{\partial z}[i] = \frac{2(V[i+1] - V[i])}{\triangle h}, \quad \text{for } i = 0, 1, \cdots, N,\\ &\frac{\partial \tau}{\partial z}[i] = \frac{2(\tau[i] - \tau[i-1])}{\triangle h}, \quad \text{for } i = 1, 2, \cdots, N.\end{aligned}$$

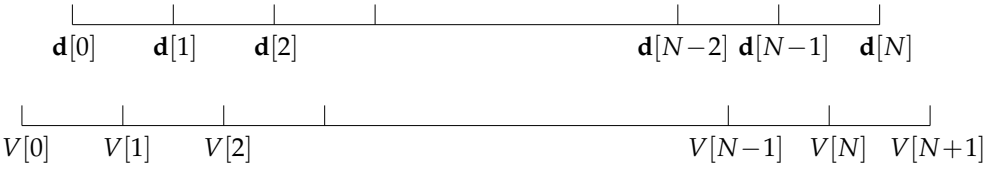

Figure 2: The staggered mesh.

Luckily, here we do not have to regain the values of **d** on the half points or the values of V on the integer points since each term involved has been presented using formulas above.

4 Numerical results

Before investigating the molecular motion, we first find the appropriate area for the penalty parameter ϵ in **f(d)**. It is proved that the discrete energy will decline if the discrete equations are solved exactly. However, to avoid computational error, we have to pay special attention on ϵ; this issue will be discussed in Section 4.1. Then we begin our investigation on **d** in Section 4.2. We get some numerical results showing that the molecules tend to tumble stating from the boundary layer and then on inner layer after a longer time period. We also test the effect of some parameters. When the viscosity μ of the flow becomes larger, we can see the tumbling rising from boundary layer then deep into the middle area more clearly. We also give a comparison of our results to some theoretical results, which indicates that the velocity gradient is the direct driving factor of the tumbling phenomena.

4.1 Penalty parameter ϵ and the energy law

In this section, we wish to find out the appropriate values for the penalty parameter ϵ. We have already shown that the discrete energy will decline provided that all the discrete equations are solved accurately. However, the discrete equations can not be solved exactly due to numerical errors. Since the $\mathbf{f}(\mathbf{d})$ term contains a factor of ϵ^{-2}, we first check this penalty parameter. We set $N=100$, $\triangle h=0.031416$, $Err=10^{-10}$, $\triangle t=10^{-5}$, $\partial_y P$=0, $\mu=0.1$, $\gamma=0.01$, $\lambda=0.005$, $\alpha=0.22$, which ensures that $\gamma\triangle t<\epsilon^2$. After some tests, we can see that ϵ is critical to guarantee the declining of the discrete energy. When $\epsilon=10^{-4}$, $f(\mathbf{d})$ increase dramatically and then the code breaks down. Fig. 3 presents two figures of the

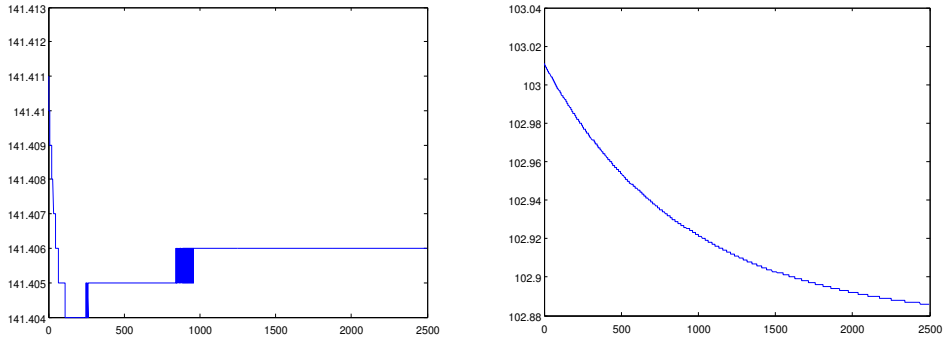

Figure 3: The energy evolution. Left: $\epsilon=0.01$, right: $\epsilon=0.05$, where the horizontal axis is the time while the vertical axis is the energy.

energy with respective to t, which corresponds to $\epsilon=0.01$, $\epsilon=0.05$.

From above, we can see that when ϵ is relatively small (when all the other parameters are fixed), the energy will not decline, or even dramatically goes up and down even when we take $\partial_y P=0$. This shows that the numerical accuracy is somehow proportional to $1/\epsilon$. So we fix ϵ to be around 0.05 or even a little bit larger according to other parameters. Without specific explanations, all our examples in the following ensure the energy declining.

4.2 Tumbling results for molecule direction d

In this subsection, we will investigate the motion of the director **d**.

We take the time step as $\triangle t$= 5e-4. Other parameters are set as: $\triangle h=0.06284$, $\partial_y P=1e6$, $T=100$, $\mu=0.1$, $\gamma=0.01$, $\lambda=0.00050$, $\alpha=0.5$, and $\epsilon=0.05$. Initial conditions are $V=0$, $(d_2,d_3)=(\cos z,\sin z)$. It is seen that there is the tumbling of several time periods on the boundary as shown in Fig. 4.

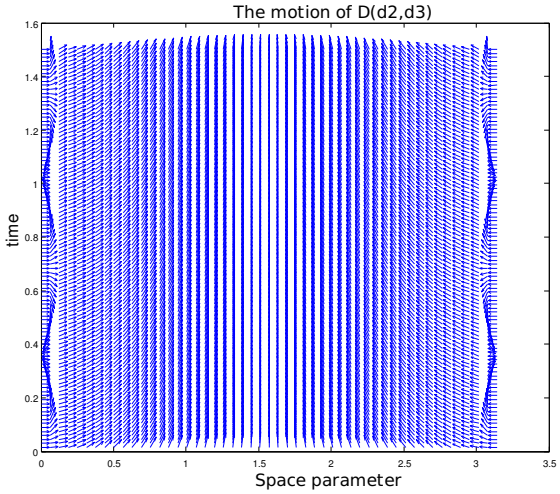

Figure 4: Motion of (d_2,d_3), where the horizontal axis is space parameter while the vertical axis is the time. Here a clear tumbling layer appears in the neighbor of the boundary.

We tend to understand the long time behavior of the molecules by choosing larger values of the time period T. However, as T becomes larger, it is difficult to recognize the detailed patterns due to the limitation of the resolution of the overall image. We can just vaguely observe that there may be a second layer where the molecules would tumble. Luckily, our assumption is confirmed by enlarging the viscosity coefficient μ. In fact, for most complex fluids, their viscosity coefficient may be very large. Now we enlarge μ and check what will happen. We can see the arrangement of **d** will be experiencing huge change as μ grows significantly. This implies that the macro fluid is really powerful to have an impact on the microstructure of the liquid crystal solvent. In the remaining

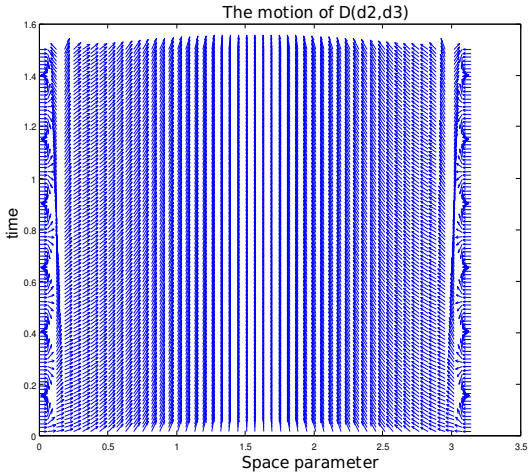

Figure 5: The motion of **d** when $\mu=1$, $\alpha=0.5$. It is observed that the distance between the second layer and the third layer is changing with time.

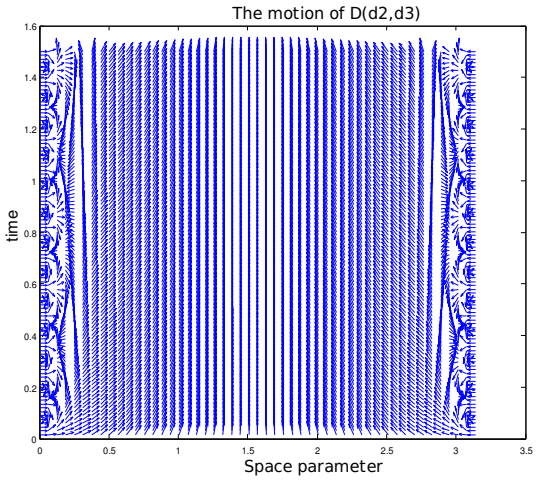

Figure 6: The motion of **d** when $\mu=10$. Here the inner tumbling layer is shown very clearly.

figures of this subsection, to focus on μ we set T=100, $\triangle h$=0.06284, $\triangle t$=0.0004, $\partial_z P$=1e6, γ=0.01, $\lambda=0.0005$, $\epsilon=0.05$.

Fig. 5 corresponds to $\mu=1$, $\alpha=0.5$. It is observed that the distance between the second layer and the third layer is changing with time. We can see that the inner layer of tumbling begins to appear.

Fig. 6 presents the motion of **d** as $\mu=10$ and $\alpha=0.5$. It is seen that the inner tumbling layer is shown very clearly.

When $\mu=100$, $\alpha=0.3$, Fig. 7 shows that the tumbling of **d** grows stronger while the total length of **d** is being distorted. The tumbling pattern grows even more complex. Also we can see the director is enduring huge distortion. There are points where the norm of

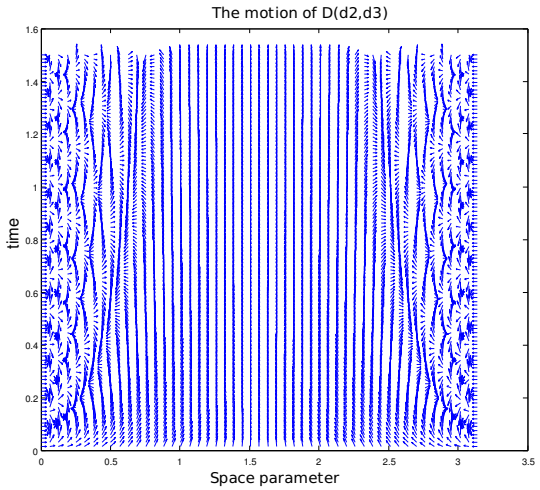

Figure 7: The motion of **d** when $\mu=100$. The tumbling pattern becomes more complex.

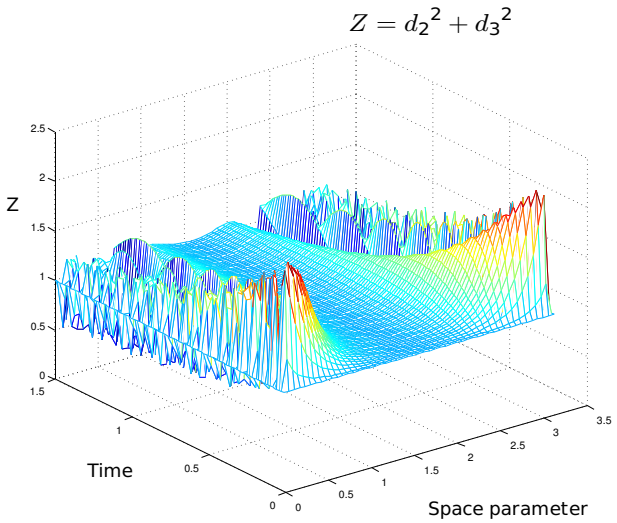

Figure 8: The norm of **d**. Some oscillations of the norm of the molecular director can be observed.

director shrinks below 1 while some other points show that the norm of the director exceeds 1 by large extent, see Fig. 8.

4.3 The behavior of V and the driving factor for tumbling

The profile of V is similar in most of the previous numerical solutions in Section 4.2. A typical case is plotted in Fig. 9.

In our numerical examples, however, when we chose $\gamma=0$, we can see each point tumble with different time period, which is really a long time for inner point. From the

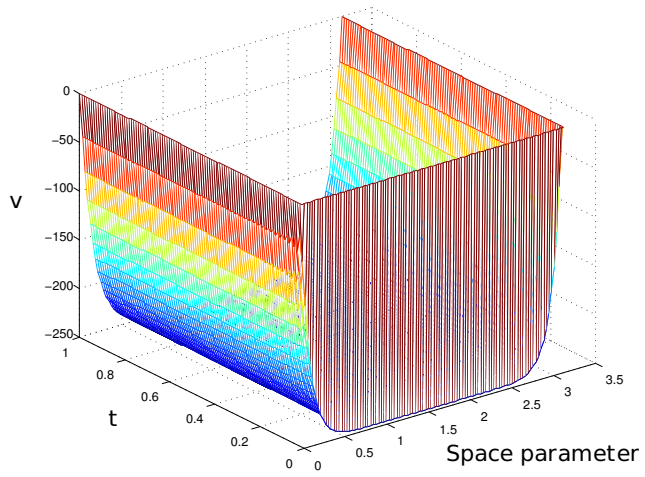

Figure 9: The profile of V, the horizontal axis is time while the vertical axis is the velocity.

theoretical analysis earlier, we assumed that $\partial_z V = \omega > 0$, which is not the case in our numerical examples. From the profile of V in Fig. 9 we can clearly see that the gradient of velocity $\partial_z V$ does not equal to zero only on the boundary layer for small viscosity μ. When μ grows larger, the supporting area for $\partial_z V$ will extend into the inner area. So the gradient of velocity is a kind of driven factor to make the director tumble. We can say that μ is powerful to make tumbling happen, however, its power stems from its impact on $\partial_z V$ which direct decides the tumbling of $\mathbf{d}$.

5 Conclusions

In this work, we have made some numerical investigations on the nonlinear system (1.1)-(1.4) in the "1+2" dimension case. We constructed a finite difference scheme paralleled to the C^0 finite element form in [17]. Our scheme satisfies a corresponding discrete energy law, which uses less computational cost than the finite element approach. We use the fixed point iteration during the linearization and realize the algorithm on a staggered mesh. We find the appropriate interval of penalty parameter ϵ to ensure that the discrete energy declines. Then we give some numerical examples which show that the molecules will tumble first on the boundary layer and later on the inner layer with a much longer time period. We also notice that the tumbling phenomena can be observed more clearly when the viscosity coefficient μ becomes larger. It is also found that the gradient of velocity is a direct driving factor through a comparison with the theoretical analysis given in Section 1.

We present a discrete energy law which is of great importance both theoretically and numerically. Theoretically, it is a natural instinct of this system which should be pre-

served by the discrete scheme. The induced tensor τ term shows the impact of the microstructure of molecules on the fluid while the coupled term of velocity and director shows impact of the fluid on the molecules. These interaction terms should annihilate according to the Newton's third law. But compared to the energy law in [17], we have an extra $(\partial_y P \cdot V)_l$ term in our equality since we assume $\partial_y P$ is a constant instead of a system variable in our model. Thus the term $(\partial_y P \cdot V)_l$ will appear to measure the external impact. When the imposed pressure gradient $\partial_y P$ equals to zero, the energy law indicates that the isolated system is dissipative. Numerically, it is a criterion for us to recognize whether we are giving the right numerical solution for the complex discrete system. Even when $\partial_y P$ does not equal to zero, in our numerical tests, if we take the initial zero condition for velocity, the term $(\partial_y P \cdot V)_l$ stays positive which accelerates the declining of the total energy. The numerical tests show that the solution is weird when the discrete energy does not decline. So we use energy declining to check whether the discrete system is appropriately solved or whether our parameters are well chosen.

Based on the tumbling patterns of **d**, we find out that the molecules on the boundary layer will tumble first while molecules on the inner layer would also join but after a longer time period. The period of tumbling is related to the viscosity μ of the flow. The larger μ will drive more molecules in the inner area to tumble and hasten their tumbling periods. The norm of the director **d** endures more violent change as well. We point out by theoretical analysis that **d** will uniformly tumble based on the assumption that $\partial_z V$ is a positive constant. However, here $\partial_z V$ varies on each point which explains the molecules have different tumbling periods. Numerical simulation shows that different μ values will lead to a change of $\partial_z V$. We then conclude that the gradient of velocity is a direct driving factor for tumbling.

Acknowledgments

The authors are very grateful to Professor Chun Liu for his helpful discussions and useful suggestions. Hui Zhang's research is partially supported by the Key Basic Research Project of the Ministry of Education of China under Grant No. 107016 and the State Key Basic Research Project of China under Grant No. 2005CB321704.

References

[1] R. Cohen, S. Y. Lin and M. Luskin, Rexation and gradiet methods for molecular orientation in liquid crystals, Comput. Phys. Commun., 53 (1989), 455-465.

[2] M. Doi and S. F. Edwards, The Theory of Polymer Dynamics, Oxford University Press, New York, 1986.

[3] M. Doi, T. Shimada and K. Okano, Concentration fluctuation of stiff polymers II -dynamical structure factor of rodlike polymers in the isotropic phase, J. Chem. Phys., 88 (1988), 4070-4075.

[4] Q. Du, B. Y. Guo and J. Shen, Fourier spectral approximation to a disspative system modeling the flow of liquid crystals, SIAM J. Numer. Anal., 39 (2001), 735-762.
[5] J. Ericksen, Convervation laws for liquid crystals, Trans. Soc. Rheol., 5 (1961), 22-34.
[6] P. G. de Gennes and J. Prost, The Physics of Liquid Crystals, 2nd ed., Oxford Science Publications, Oxford, 1993.
[7] R. Glowinski, P. Lin and X. B. Pan, An operator-splitting method for a liquid crystal model, Comput. Phys. Commun., 152 (2003), 242-252.
[8] R. Glowinski and P. Le Tallec, Augmented Lagrangian and Operator-Splitting Methods in Nonlinear Mechanics, SIAM, Philadelphia, 1989.
[9] S. Z. Hess, Fokker-Planck-equation approach to flow alignment in liquid crystals, Z. Naturforsch., 31A (1976), 1034-1037.
[10] G. B. Jeffery, The motion of ellipsoidal particles immersed in a viscous fluids, Roy. Soc. Lond. Proc. Ser. A, 102 (1922), 161-179.
[11] N. Kuzuu and M. Doi, Constitutive equation foe nematic liquid crystals under weak velocity gradient derived from a molecular kinetic equation, J. Phys. Soc. Jpn., 52 (1983), 3486-3496.
[12] M. Lees, A priori estimates for the solutions of difference approximations to parabolic partial differential equations, Duke Math. J., 27 (1960), 297-311.
[13] F. H. Lin and C. Liu, Nonparabolic dissipative systems, modeling the flow of liquid crystals, Commun. Pure Appl. Math., 48 (1995), 501-537.
[14] F. H. Lin and C. Liu, Global existence of solutions for Ericksen-Leslie system, Arch. Rat. Mech. Anal., 154 (2001), 135-156.
[15] F. H. Lin, C. Liu and P. Zhang, On viscoelastic fluids, Commun. Pure Appl. Math., 58 (2005), 1-35.
[16] P. Lin and C. Liu, Simulation of singularuty dynamics in liquid crystal flows: a C^0 finite element approach, J. Comput. Phys., 215 (2006), 348-362.
[17] P. Lin, C. Liu and H. Zhang, An energy law preserving C0 finite element scheme for simulating the kinematic effects in liquid crystal flow dynamics, J. Comput. Phys., 227 (2007), 1411-1427.
[18] C. Liu and N. J. Walkington, Mixed methods for the approximation of liquid crystal flows, M2AN, 36 (2002), 205-222.
[19] C. Liu and N. J. Walkington, An Eulerian description of fluids containing visco-hyperelastic particles,, Arch. Ration. Mech. Anal., 159 (2001), 229-252.
[20] C. Liu, J. Shen and X. Yang, Dynamics of defect motion in nematic liquid crystal flow: modeling and numerical simulation, Commun. Comput. Phys., 2 (2007), 1184-1198.
[21] W. Maier and A. Saupe, A simple molecular statistical theory of the nematic crystalline-liquid phase, I. Z. Naturforsch, 14A (1959), 882-889.
[22] G. Marrucci and F. Greco, The elastic constants of Maier-Saupe rodlike molecule nematics, Mol. Cryst. Liq. Cryst., 206 (1991), 17-30.
[23] L. Onsager, The effects of shape on the interaction of collodial particles, Ann. N. Y. Acad. Sci., 51 (1949), 627-659.
[24] Q. Wang, A hydrodynamic theory for solutions of nonhomogeneous nematic liquid crystalline polymers of different configurations, J. Chem. Phys., 116 (2002), 9120-9136.
[25] Q. Wang, M. G. Forest and R. Zhou, A kinetic theory for solutions of nonhomogeneous nematic liquid crystalline polymers with density variations, J. Fluids Eng., 126 (2004), 180-188.